PCCP

ROYAL SOCIETY OF CHEMISTRY

PAPER

View Article Online
View Journal | View Issue

Cite this: *Phys. Chem. Chem. Phys.*, 2022, **24**, 15912

High-performance Ruddlesden–Popper two-dimensional perovskite solar cells *via* solution processed inorganic charge transport layers†

Zhihai Liu,[a] Lei Wang,[b] Xiaoyin Xie,[c] Chongyang Xu,[d] Jianfeng Tang*[e] and Wei Li*[e]

Received 4th May 2022,
Accepted 6th June 2022

DOI: 10.1039/d2cp02033e

rsc.li/pccp

Two-dimensional (2D) layered halide perovskites have been shown to enable improved long-term stability in comparison to the well-known three-dimensional hybrid organic–inorganic halide perovskites. The optoelectronic properties of the 2D perovskites are strongly influenced by the chemical nature of the charge transport layer. In this work, we fabricated Ruddlesden–Popper 2D perovskite solar cells (PSCs) using solution processed inorganic NiO_x and a $C_{60}:C_{70}$ (1 : 1) mixture as the hole and electron transport layers, which significantly improved the performance of the 2D PSCs. Time resolved photoluminescence measurements indicate the shortened lifetime of excitons, which demonstrates the excellent charge extraction properties. The PSCs based on these inorganic charge transport materials (CTMs) exhibit an average power conversion efficiency (PCE) of 14.1%, which is higher than that (12.3%) of PSCs using organic CTMs of poly(3,4-ethylenedioxythiophene) : poly(styrenesulfonate) (PEDOT:PSS) and phenyl-C61-butyric acid methyl ester (PCBM). Compared with PEDOT:PSS and PCBM based cases, the PSCs using inorganic CTMs also show improved long-term stability, with the PCE degradation significantly suppressed from 20% to 12% after a measurement of 15 days. The best PSCs using NiO_x and $C_{60}:C_{70}$ show a high PCE of 14.4%, with a stable power output and negligible hysteresis.

1. Introduction

Recently, organometallic halide perovskite materials have been intensively investigated owing to their unique advantages for optoelectronic applications, such as sufficient light absorption, high charge carrier mobilities, direct band-gaps and solution processibility.[1–4] As a result, the power conversion efficiency (PCE) of perovskite solar cells (PSCs) has been significantly improved to 25.5%, which is comparable to that of silicon solar cells.[5] In the structure of PSCs, the perovskite absorbers are usually sandwiched between the hole transport layer (HTL) and the electron transport layer (ETL), which further connect with the anode and the cathode.[3] For regular n–i–p PSCs, 2,2′,7,7′-tetrakis-(*N*,*N*-di-*p*-methoxyphenylamine)-9,9′-spirobifluorene (spiro-OMeTAD) and TiO_2 are widely used as the HTL and ETL, respectively,[6–8] while for inverted p–i–n PSCs, usually organic poly(3,4-ethylenedioxythiophene) : poly(styrenesulfonate) (PEDOT:PSS) and phenyl-C61-butyric acid methyl ester (PCBM) are used as the hole and electron transport materials, which can be simply deposited through a spin coating operation.[6,9,10] However, conventional PSCs using $MAPbX_3$ (MA and X strand for CH_3NH_3 and halogen) always suffer from a serious problem of poor stability, which is detrimental for commercial applications of PSCs.[11,12]

To overcome this problem, developing new perovskite absorbers and charge transport materials (CTMs) with higher intrinsic stability becomes an important aspect. In case of absorbers, recently Ruddlesden–Popper 2-dimensional (2D) perovskites have been widely used for fabricating PSCs because of their tunable band-gaps and better stability.[13–16] For example, the $(BA)_2(MA)_{n-1}Pb_nI_{3n+1}$ (BA = $CH_3(CH_2)_3NH_3$) perovskite series showed direct band-gaps between 1.5 and 2.2 eV,[17] which is applicable for fabricating PSCs with high PCE and superior stability. For CTMs, conventional spiro-OMeTAD, PEDOT:PSS and PCBM are organic materials, which show a relatively low stability in air.[18–20] Although TiO_2 is an inorganic electron

[a] *School of Physics and Electronic Information, Yantai University, Yantai 264005, China*
[b] *School of Artificial Intelligence, Beijing Technology and Business University, Beijing, 100048, China*
[c] *School of Chemistry and Chemical Technology, Hubei Polytechnic University, Huangshi 435003, China*
[d] *Yantai Research Institute and Graduate School of HEU, Harbin Engineering University, Harbin 150001, China*
[e] *School of Chemistry and Materials Science, Hunan Agricultural University, Changsha 410128, China. E-mail: weili@hunau.edu.cn, jftang@hunau.edu.cn*

† Electronic supplementary information (ESI) available: Additional figures and table. See DOI: https://doi.org/10.1039/d2cp02033e

transport material with excellent stability, the photocatalytic effect of TiO_2 could decompose perovskite into PbI_2 under the irradiation of ultraviolet light.[21] As a result, some inorganic CTMs have been investigated for improving the stability of PSCs. For example, solution processed NiO_x has been widely used as the HTL in PSCs, which is a typical p-type semiconductor with suitable energy levels.[22,23] Compared with PEDOT:PSS, PSCs with NiO_x showed a superior performance with comparable PCEs and enhanced stability.[24–26] Moreover, n-type ZnO and SnO_2 are good electron transport materials for replacing TiO_2 in PSCs, which could simultaneously improve PCE and stability of PSCs.[27,28] Liu and co-workers used inorganic HTL (NiO_x) and ETL (ZnO/C_{60}) for fabricating $CsPbI_2Br$-based PSCs, which showed an excellent PCE of 13.3% and enhanced stability.[29] Pristine fullerenes (C_{60} or C_{70}) show higher electron mobilities than fullerene derivatives (such as PCBM), which are good candidates for ETLs in PSCs.[30] Although each individual fullerene shows a poor solubility, the mixture of several fullerenes can be well dissolved in organic solvents at high concentrations due to the increased configurational entropy.[30,31] As a result, the film of fullerene mixture can be deposited through a solution process (such as spin-coating or spray coating) with a uniform morphology. For example, Lin *et al.* and Xu *et al.* reported the use of a fullerene mixture (containing C_{60} or C_{70}) as ETLs in regular and inverted $MAPbX_3$-based PSCs, achieving high PCEs of 16.7–16.9% with improved stability.[31,32] Considering the stability problem, it is very important to investigate the use of an inorganic HTL and ETL in 2D PSCs and their effect on the performance.

In this study, we introduce the use of inorganic solution processable HTL (NiO_x) and ETL (fullerene mixture, $C_{60}:C_{70}$ = 1:1) in the fabrication of Ruddlesden–Popper type 2D PSCs. Compared with the use of conventional PEDOT:PSS and PCBM, using NiO_x and fullerene mixture could improve the charge transport property, which is beneficial for improving the performance of PSCs. As a result, the PSCs based on NiO_x and the fullerene mixture exhibited an average PCE of 14.1%, which is much higher than that (12.3%) of PEDOT:PSS and PCBM based PSCs. Based on this technique, stability of the PSCs was also improved with a significantly suppressed PCE degradation from 20% to 12% after a measurement of 15 days. This was mainly induced from the intrinsic high stability of well-crystallized perovskite and inorganic CTMs (NiO_x and pristine fullerenes). The highest PCE of 14.4% was achieved for PSCs using NiO_x and the fullerene mixture with a stable power output and negligible hysteresis. Our results demonstrate that using inorganic NiO_x and the fullerene mixture as the CTMs is an effective approach for boosting the performance of Ruddlesden–Popper 2D PSCs.

2. Experimental section

2.1 Device fabrication

Fullerenes (C_{60} and C_{70}) and PEDOT:PSS (P VP AI4083) were purchased from Nano-C Inc. (USA) and Heraeus Clevios (Germany), respectively. Methylammonium iodide (MAI) and fluorine-doped tin oxide (FTO) glasses were purchased from Advanced Election Technology Co., Ltd (China). Butylammonium iodide (BAI), $Ni(Ac)_2{\cdot}4H_2O$, *N,N*-dimethylformamide (DMF), dimethyl sulfoxide (DMSO) and *o*-dichlorobenzene (*o*-DCB) were purchased from Sigma-Aldrich (USA). PbI_2 and bathocuproine (BCP) were purchased from Xi'an Polymer Light Technology Corp. (China). As shown in Fig. 1(a), the PSCs were fabricated following a structure of glass/FTO/NiO_x/

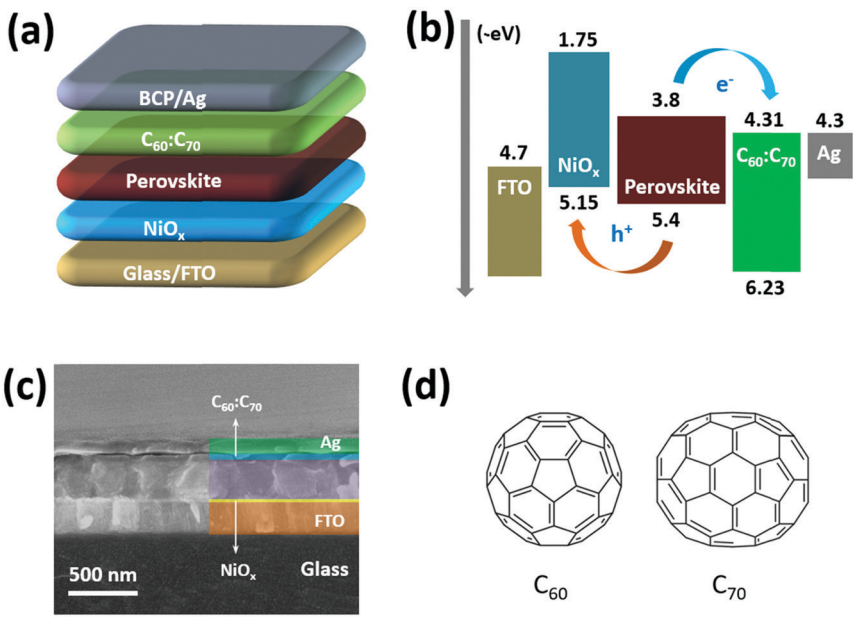

Fig. 1 (a) Schematic device structure of the PSCs; (b) schematic energy levels of the functional layers involved in the PSCs; (c) cross-sectional SEM image of a PSC; (d) molecular structures of C_{60} and C_{70}.

$(BA)_2(MA)_3Pb_4I_{13}/C_{60}:C_{70}$/BCP/Ag. First, 0.1 mmol $Ni(Ac)_2\cdot 4H_2O$ and 6 μL ethanolamine were dissolved in 1 mL 2-methoxyethanol, which was further stirred at 70 °C overnight. The NiO_x precursor was spin coated onto the FTO glasses at 3500 rpm, followed by a thermal annealing at 400 °C for 1 h in air. Then the perovskite precursor (containing BAI : MAI : PbI_2 = 2 : 3 : 4 in a mixed-solvent of DMF and DMSO) was spin coated onto the NiO_x layers at 4000 rpm in a N_2 filled glovebox. The $(BA)_2(MA)_3Pb_4I_{13}$ perovskite films were formed after being heated at 100 °C for 10 min. Next, a fullerene mixture solution ($C_{60}:C_{70}$ = 1 : 1 in *o*-DCB at 30 mg mL^{-1}) was spin coated onto the perovskite films at 1000, 2000 or 3000 rpm for 30 s. After that, the BCP solution (in propanol at 0.5 mg mL^{-1}) was spin coated on the samples at 4500 rpm. For control PSCs, PEDOT:PSS was spin coated onto the FTO substrates at 4500 rpm and annealed at 150 °C for 10 min. PCBM solution (30 mg mL^{-1} in *o*-DCB) was spin coated at 2000 rpm onto the perovskite films. Finally, the Ag electrodes of about 100 nm were thermally evaporated onto the samples under a high vacuum of 10^{-4} Pa to form an effective working area of 0.1 cm^2 for the PSCs, which was defined by a shadow mask.

2.2 Characterization

The X-ray diffraction (XRD) spectra were measured using an X-ray diffractometer (Panalytical, the Netherlands). The cross-sectional image of the PSCs and top-view images of the surfaces were acquired using an SU8020 scanning electron microscope (SEM, Hitachi, Japan), which was operated at an acceleration voltage of 8 kV. The photoluminescence (PL) spectra of the films were measured using a spectrometer (FLS920, Edinburgh Instruments, UK), with the excitation wavelength of 372 nm and power density of 9 mW cm^{-2}. The energy levels of NiO_x and fullerene mixture were measured using an ultraviolet photoelectron spectroscope (UPS) with the incident light energy of 21.22 eV. The electrochemical impedance spectroscopy (EIS) spectra of the PSCs were performed using an electrochemical work station (Bio-Logic, France). The current density–voltage (*J*–*V*) characteristics of the PSCs were measured under an irradiation intensity of 100 mW cm^{-2} (AM1.5). The incident photon-to-current efficiency (IPCE) spectra of the PSCs were measured using a solar cell IPCE measurement system (Solar Cell Scan 100, Zolix, China).

3. Results and discussion

Fig. 1(b) shows the schematic energy alignment of all the functional layers involved in the PSCs, which illustrates the charge transport process under the irradiation of sunlight. As shown in Fig. S1, (ESI†) the valence band of NiO_x is about −5.15 eV, which is slightly higher than highest occupied molecular orbital (HOMO, −5.4 eV) level of the $(BA)_2(MA)_3Pb_4I_{13}$ perovskite and lower than the work function (−4.7 eV) of FTO. The conduction band of fullerene mixture ($C_{60}:C_{70}$) is about −4.31 eV (calculated from Fig. S2, ESI†), which is lower than the lowest unoccupied molecular orbital (LUMO, −3.8 eV) level of perovskite and similar to the work function (−4.3 eV) of the Ag electrode. As a result, the energy levels of NiO_x and fullerene mixture are suitable for charge extraction and transportation from the perovskite absorber to electrodes. Fig. 1(c) presents the cross-sectional SEM image of the PSCs using NiO_x and fullerene mixture, which clearly shows a dense layer-by-layer structure. From the SEM image, the thicknesses of NiO_x, perovskite and $C_{60}:C_{70}$ layers are about 15, 420 and 40 nm, respectively, which are typical values for PSCs with high performance.[13–16,31] The molecular configurations of C_{60} and C_{70} are shown in Fig. 1(d), which only contains C–C bonding without other chemical groups.

Fig. 2(a) presents the *J*–*V* characteristics the PSCs using PEDOT:PSS/PCBM and $NiO_x/C_{60}:C_{70}$ as the charge transport layers, with the device parameters summarized in Table 1. The control PSCs using PEDOT:PSS and PCBM show an average PCE of 12.3%, with an open-circuit voltage (V_{oc}) of 1.02 V, a short-circuit current density (J_{sc}) of 17.6 mA cm^{-2} and a fill factor (FF) of 68.6%. The performance of the control devices is similar with that in previous studies based on $(BA)_2(MA)_3Pb_4I_{13}$ perovskite,[13–17] indicating the good optimization of our experiment. Upon using inorganic NiO_x and fullerene mixture, the average PCE of the PSCs was significantly improved to 14.1%, with J_{sc} and FF simultaneously improved to 18.9 mA cm^{-2} and 73.8%. The V_{oc} was slightly decreased to 1.01 V, which might be induced by the energy levels of NiO_x and pristine fullerenes.[31] As shown in Fig. S1 and Table S3, (ESI†) 2000 rpm is an optimal speed for the spin coating of fullerene mixture, which results in the best performance of the PSCs. The PCE variations are shown in Fig. S4, (ESI†) which indicate a stable *J*–*V* performance for each batch of the PSCs using different charge transport layers. Fig. 2(b) shows the IPCE spectra of the two kinds of PSCs, from which integrated J_{sc} can be obtained. The calculated J_{sc} values from the IPCE spectra are 17.2 and 18.5 mA cm^{-2} for PSCs using PEDOT:PSS/PCBM and $NiO_x/C_{60}:C_{70}$, which are within 2.5% different from those obtained in the *J*–*V* performance. From Fig. 3(c), the best performing PSC using $NiO_x/C_{60}:C_{70}$ shows a high PCE of 14.4%, which is an excellent value for $(BA)_2(MA)_3Pb_4I_{13}$ based 2D PSCs.[13–17,33–35] By reverse scanning, the PCE becomes slightly larger to 14.9%, indicating a small hysteresis of the PSCs. The difference from the *J*–*V* performance is mainly induced by the slightly increased FF (75.2%) and V_{oc} (1.05 V) whereas for PEDOT:PSS/PCBM based PSCs shown in Fig. S5, (ESI†) the reverse scanning PCE is 13.5%, which indicates a larger hysteresis. The suppressed hysteresis degree may be induced by the fewer defects in the PSCs upon using NiO_x and $C_{60}:C_{70}$, which will be discussed later. Fig. 2(d) shows the steady state power output for the best performing PSCs, which displays a stable J_{sc} and PCE for 300 s. The J_{sc} stabilizes between a range of 16.2 to 16.4 mA cm^{-2}, resulting in a PCE output of 14.0–14.1%.

To identify the reason for the performance improvement upon using NiO_x and the fullerene mixture, we measured the morphology of the perovskite $(BA)_2(MA)_3Pb_4I_{13}$ perovskite films formed on different underlying HTLs. From Fig. 3(a and b), both the perovskite films formed on PEDOT:PSS and NiO_x

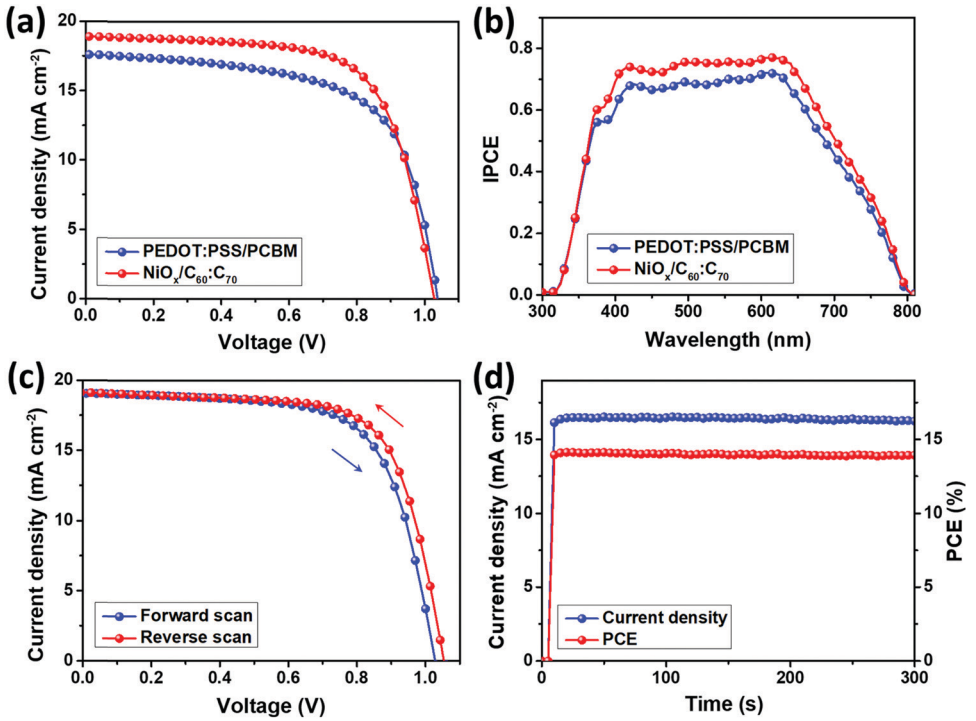

Fig. 2 Forward scanning J–V characteristics (a) and IPCE spectra (b) of the PSCs using PEDOT:PSS/PCBM and $NiO_x/C_{60}:C_{70}$ as the charge transport layers; (c) forward and reverse scanning J–V characteristics of a best performing PSC using NiO_x and $C_{60}:C_{70}$ as the HTL and ETL; and (d) current density and PCE as a function of time for the best performing PSC under a bias of 0.86 V.

Table 1 Device parameters (average values of 16 individual PSCs) for the PSCs using PEDOT:PSS/PCBM and $NiO_x/C_{60}:C_{70}$ as the charge transport layers

HTL/ETL	V_{oc} (V)	J_{sc} (mA cm^{-2})	FF (%)	PCE (%)	Best PCE (%)
PEDOT:PSS/PCBM	1.02 ± 0.01	17.6 ± 0.3	68.6 ± 1.5	12.3 ± 0.3	12.6
$NiO_x/C_{60}:C_{70}$	1.01 ± 0.01	18.9 ± 0.3	73.8 ± 1.3	14.1 ± 0.3	14.4

HTLs show a uniform morphology with a full surface coverage, which is consistent with those existing in previous studies.[14–16] However, the perovskite film formed on NiO_x showed enlarged perovskite planes and reduced quantity of pinholes, indicating an improved quality of the $(BA)_2(MA)_3Pb_4I_{13}$ film. Fig. 3(c) shows the XRD patterns of the two perovskite films on PEDOT:PSS and NiO_x, which clearly reveals the crystallinity information for the films. There are two dominant peaks at 14.2° and 28.5°, which represent the crystallographic (111) and (202) planes for the $(BA)_2(MA)_3Pb_4I_{13}$ film.[15] For the NiO_x based perovskite film, these characteristic peaks become higher and sharper than those of the perovskite on PEDOT:PSS. The full width at half maximum (FWHM) of the (202) peak for the NiO_x based perovskite film is 0.208°, which is narrower than FWHM (0.232°) of the perovskite on PEDOT:PSS. This indicates the improved crystallinity of the perovskite film formed on NiO_x. Fig. S6 (ESI†) shows the absorption spectra of the perovskite films formed on NiO_x and PEDOT:PSS. The slightly higher absorption of using NiO_x is consistent with the improved quality of the perovskite film. The SEM images and XRD spectra demonstrate the improved quality of the perovskite film upon using NiO_x. This can be explained from the hydrophilic and hydrophobic nature of the underlying PEDOT:PSS and NiO_x, which could significantly influence the crystallization of the upper perovskite films. As shown in Fig. 3(d), the contact angle of NiO_x is 80°, much higher than that (12°) of PEDOT:PSS film. This indicates a more hydrophobic property of the NiO_x surface, which could induce a larger Gibbs free-energy barrier for suppressing the nucleation of the perovskite at the initial stage.[36,37] Moreover, the hydrophobic surface of NiO_x would decrease the anchoring effect of perovskite precursor, which further accelerates the movement of the perovskite boundaries at the later stage of crystal growth.[36] Consequently, crystallization of the perovskite film was improved upon using hydrophobic underlying NiO_x, which further resulted in larger perovskite planes with fewer pinholes. A well crystallized perovskite film with uniform morphology usually contains less charge trapping defects,[31] which is highly related to the improved PCE and suppressed hysteresis. From Fig. S7, (ESI†) the SEM images of NiO_x and fullerene mixture both show a smooth morphology without significant aggregations, which is beneficial for forming ohmic contact with other functional layers.

The charge transport property of the PSCs can be revealed from the PL spectra and EIS measurements. As shown in Fig. 4(a), the bare $(BA)_2(MA)_3Pb_4I_{13}$ perovskite (on glass)

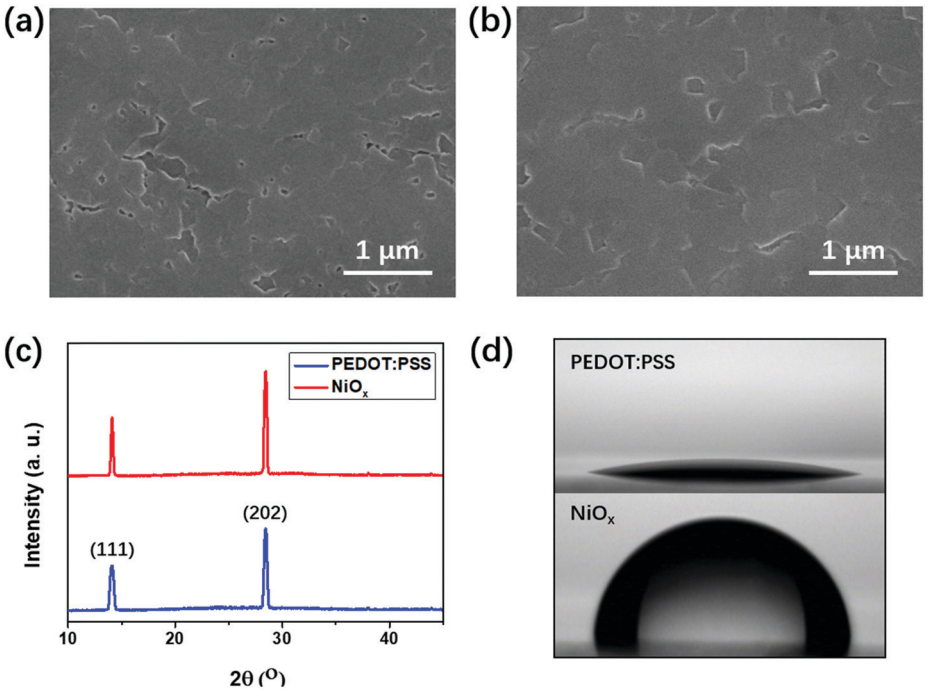

Fig. 3 SEM images of the $(BA)_2(MA)_3Pb_4I_{13}$ perovskite films formed on (a) PEDOT:PSS and (b) NiO_x; (c) XRD patterns of the perovskite films formed on PEDOT:PSS and NiO_x; and (d) contact angles of water drops on the surfaces of PEDOT:PSS and NiO_x films.

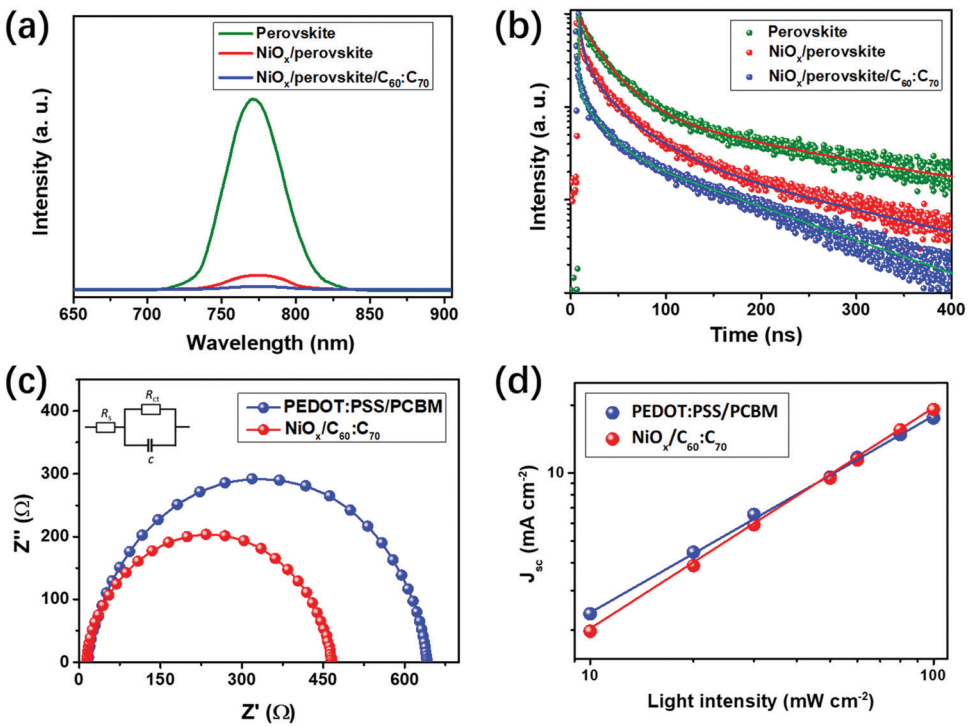

Fig. 4 PL (a) and time resolved PL (TR-PL) (b) spectra of bare perovskite, NiO_x/perovskite and NiO_x/perovskite/C_{60}:C_{70} films; (c) EIS spectra of the PSCs using PEDOT:PSS/PCBM and $NiO_x/C_{60}:C_{70}$ as the charge transport layers; and (d) light intensity dependence of J_{sc} for PSCs using PEDOT:PSS/PCBM and $NiO_x/C_{60}:C_{70}$ as the charge transport layers.

exhibits a strong PL signal at 776 nm, which is similar with that in previous studies.[15,38] The PL signal of the perovskite on NiO_x was dramatically quenched by about 90%, indicating the excellent hole extraction properties of using NiO_x. When adding the

fullerene mixture as the ETL, the PL signal almost disappeared, indicating the full quenching of excitons in the perovskite absorber. Fig. 4(b) shows the time resolved PL (TR-PL) spectra of the bare perovskite, NiO_x/perovskite and NiO_x/perovskite/$C_{60}:C_{70}$ films, which reveal the lifetime of the excitons in the devices. With bi-exponential fitting to these curves, parameters of fast (τ_1) and slow (τ_1) decay times can be obtained, which represent photoluminescence quenching of free carriers and radiative recombination of trapped carriers.[34] As shown in Table S2, (ESI†) the τ_1 was significantly decreased from 32.3 to 6.8 ns and τ_2 was reduced from 304.8 to 38.2 ns upon using NiO_x and $C_{60}:C_{70}$, indicating the excellent quenching effect of excitons. The PL and TR-PL spectra for the devices of NiO_x/perovskite/$C_{60}:C_{70}$ and PEDOT:PSS/perovskite/PCBM are shown in Fig. S8 (ESI†). Compared with the use of PEDOT:PSS and PCBM, using NiO_x and $C_{60}:C_{70}$ exhibited a lower PL intensity and faster decay time, which indicates the improved charge extracting properties. From the PL and TR-PL measurements, using NiO_x and the fullerene mixture could effectively extract charge carriers from the perovskite absorber. The charge transfer property in the PSCs can be conducted from the EIS measurements. As shown in Fig. 4(c), the EIS spectra can be divided into the high (on the left) and low (on the right) frequency ranges, which reveal the series resistance (R_s) and charge transfer resistance (R_{ct}) of the PSCs.[38,39] The R_s and R_{ct} values can be obtained by fitting the EIS spectra using the equivalent circuit shown in the inset, which contains these parameters. The R_s and R_{ct} are highly related to the contact resistance of different layers and charge transport property in the PSCs, respectively.[38] As indicated from the fitting results, the R_{ct} of PSCs using $NiO_x/C_{60}:C_{70}$ is 425 Ω, which is lower than that (508 Ω) of PEDOT:PSS/PCBM based PSCs. This demonstrates the improved charge transport property of the PSCs upon using $NiO_x/C_{60}:C_{70}$, which is in consistent with the PL analysis. Fig. 4(d) shows the dependence of J_{sc} on the light intensity from 0.1 to 1 sun for the two kinds of PSCs. The calculated slope of $NiO_x/C_{60}:C_{70}$ based PSCs is 0.98, which is higher than that (0.93) of PEDOT:PSS/PCBM based ones. This indicates the suppressed bimolecular charge recombination in the PSCs upon using $NiO_x/C_{60}:C_{70}$.[40] This phenomenon can also be explained by the improved charge transport property upon using $NiO_x/C_{60}:C_{70}$, which weakens the charge recombination at the interfaces of NiO_x/perovskite/$C_{60}:C_{70}$. As a result, the improved performance of PSCs using $NiO_x/C_{60}:C_{70}$ can be attributed to the improved quality of perovskite absorber and enhanced charge transportation at the interfaces.

In addition, we compared the stability performance of the PSCs using PEDOT:PSS/PCBM and $NiO_x/C_{60}:C_{70}$ by storing and testing the samples for 15 days under ambient conditions (25 °C, 30–40% humidity). As shown in Fig. 5(a), the PSCs using PEDOT:PSS and PCBM maintained a PCE of 9.8% after a measurement of 15 days, which corresponded to a PCE degradation of about 20% (initial PCE = 12.3%) whereas the $NiO_x/C_{60}:C_{70}$ based PSCs showed a higher PCE of 12.4% after 15 days, leading to a lower PCE degradation of 12%. The PSCs using $NiO_x/C_{60}:C_{70}$ showed an excellent long-term stability,

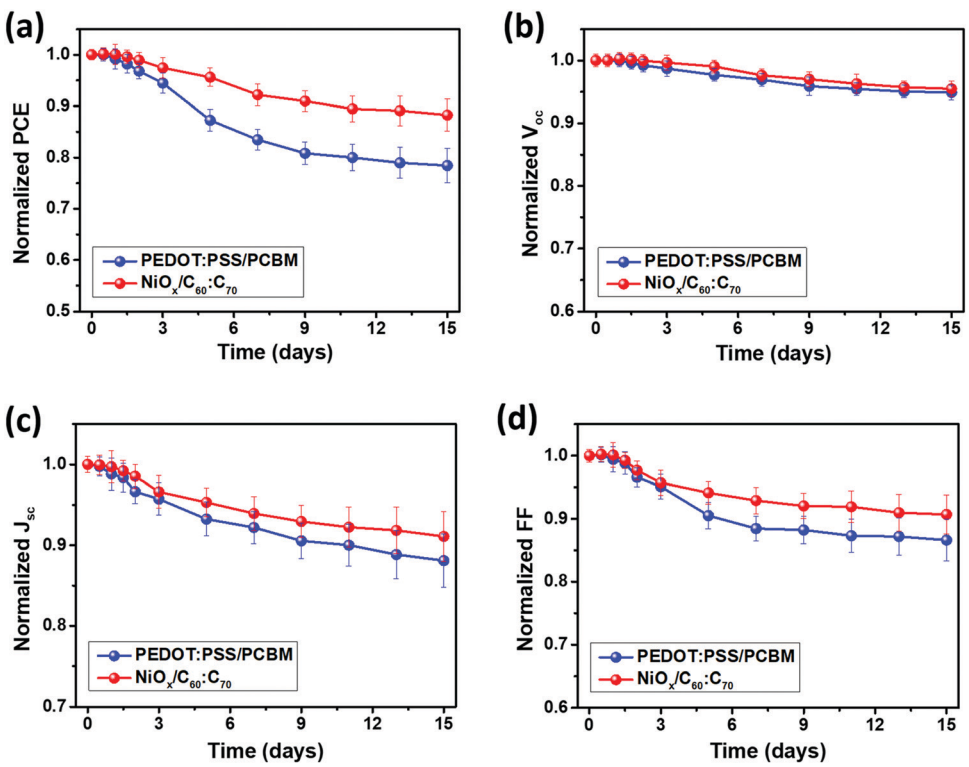

Fig. 5 Long-term stability of the PSCs using PEDOT:PSS/PCBM and $NiO_x/C_{60}:C_{70}$ as the charge transport layers, in terms of their normalized PCE (a), V_{oc} (b), J_{sc} (c) and FF (d) as a function of time.

which is better than those of using organic charge transport layers[14,15,38] in a similar condition. From Fig. 5(b–d), for both cases, the PCE degradation was mainly induced by the degraded J_{sc} and FF, which are highly related to the series and shunt resistances in the PSCs.[41] The degradation of perovskite films could induce a larger contact resistance at the interfaces and more leakage current, which would increase the series resistance and decreases the shunt resistance in PSCs. As discussed above, the perovskite film on NiO_x showed a better quality than that on PEDOT:PSS, which could induce a higher intrinsic stability of the PSCs.[31,42] On the other hand, the inorganic NiO_x and $C_{60}:C_{70}$ own better intrinsic stability than organic PEDOT:PSS and PCBM, which could more effectively protect the inner perovskite absorber.[29] Moreover, PEDOT:PSS is a hydrophilic material, which can absorb moisture from air and further decompose the perovskite.[43] As a result, using hydrophobic NiO_x as the HTL can prevent this moisture induced degradation of the PSCs, which is another reason for the improved long-term stability.

4. Conclusions

Ruddlesden–Popper 2D PSCs have been intensively studied due to the advantages of high stability and simple processability. In this work, we developed solution-processed inorganic NiO_x and fullerene mixture ($C_{60}:C_{70}$ =1 : 1) as the HTL and ETL for improving the performance of Ruddlesden–Popper 2D PSCs. Compared with PSCs using conventional PEDOT:PSS and PCBM, the $NiO_x/C_{60}:C_{70}$-based PSCs showed a significantly improved PCE of 14.1% (on average), which was induced by the improved J_{sc} and FF. Upon using NiO_x and fullerene mixture, long-term stability of the PSCs was also improved with the PCE degradation dramatically suppressed from 20% to 12% after being tested for 15 days. The SEM and XRD results demonstrate the improved film quality and crystallinity for perovskite films formed on NiO_x. The PL, EIS and light-dependent measurements indicate the excellent charge transport property of using NiO_x and fullerene mixture in the PSCs. The best performing PSC using $NiO_x/C_{60}:C_{70}$ exhibits a high PCE of 14.4%, with a stable power output and negligible hysteresis. Our result demonstrates that using solution processed inorganic NiO_x and pristine fullerenes as the CTMs is an effective way of fabricating Ruddlesden–Popper 2D PSCs with high efficiency and stability.

Conflicts of interest

There are no conflicts to declare.

Acknowledgements

This work was supported by the Hubei Polytechnic University Talent Introduction Fund (No. KJC2021HXHG01) and the National Natural Foundation of China (No. 51871067). J. F. T acknowledges funding from the Natural Science Foundation of Hunan Province (No. 2020JJ4375) and the Double First-Class Construction Project of Hunan Agricultural University (No. SYL2019063). W. L. acknowledges the Chinese Postdoctoral Science Foundation (No. 2021M701168) and the Science and Technology Innovation Program of Hunan Province (No. 2021RC3089).

References

1 M. M. Lee, J. Teuscher, T. Miyasaka, T. N. Murakami and H. J. Snaith, *Science*, 2012, **338**, 643–647.
2 A. Kojima, K. Teshima, Y. Shirai and T. Miyasaka, *J. Am. Chem. Soc.*, 2009, **131**, 6050–6051.
3 W. S. Yang, B.-W. Park, E. H. Jung, N. J. Jeon, Y. C. Kim, D. U. Lee, S. S. Shin, J. Seo, E. K. Kim, J. H. Noh and S. I. Seok, *Science*, 2017, **356**, 1376–1379.
4 S. D. Stranks, G. E. Eperon, G. Grancini, C. Menelaou, M. J. P. Alcocer, T. Leijtens, L. M. Herz, A. Petrozza and H. J. Snaith, *Science*, 2013, **342**, 341–344.
5 NREL Best Research-Cell Efficiency Chart (Photovoltaic Research). Available online: **https://www.nrel.gov/pv/cell-efficiency.html** (accessed on 13 January 2021).
6 H. Kim, K.-G. Lim and T.-W. Lee, *Energy Environ. Sci.*, 2016, **9**, 12–30.
7 L. Chen, X. Xie, Z. Liu and E.-C. Lee, *J. Mater. Chem. A*, 2017, **5**, 6974–6980.
8 D. Li, D. Zhang, K.-S. Lim, Y. Hu, Y. Rong, A. Mei, N.-G. Park and H. Han, *Adv. Funct. Mater.*, 2021, **31**, 2008621.
9 J. H. Heo, H. J. Han, D. Kim, T. K. Ahn and S. H. Im, *Energy Environ. Sci.*, 2015, **8**, 1602–1608.
10 K. Jiang, F. Wu, G. Zhang, P. C. Y. Chow, C. Ma, S. Li, K. S. Wong, L. Zhu and H. Yan, *J. Mater. Chem. A*, 2019, **7**, 21662–21667.
11 G. Liu, X. Xie, Z. Liu, G. Cheng and E.-C. Lee, *Nanoscale*, 2018, **10**, 11043–11051.
12 J. A. Christians, P. A. Miranda Herrera and P. V. Kamat, *J. Am. Chem. Soc.*, 2015, **137**, 1530–1538.
13 H. Tsai, W. Nie, J.-C. Blancon, C. C. Stoumpos, R. Asadpour, B. Harutyunyan, A. J. Neukirch, R. Verduzco, J. J. Crochet, S. Tretiak, L. Pedesseau, J. Even, M. A. Alam, G. Gupta, J. Lou, P. M. Ajayan, M. J. Bedzyk, M. G. Kanatzidis and A. D. Mohite, *Nature*, 2016, **536**, 312–316.
14 Y. Xie, H. Yu, J. Duan, L. Xu and B. Hu, *ACS Appl. Mater. Interfaces*, 2020, **12**, 11190–11196.
15 Z. Liu, L. Wang, C. Xu and X. Xie, *Sustainable Energy Fuels*, 2021, **5**, 2595–2601.
16 X. Zhang, X. Ren, B. Liu, R. Munir, X. Zhu, D. Yang, J. Li, Y. Liu, D. Smilgies, R. Li, Z. Yang, T. Niu, X. Wang, A. Amassian, K. Zhao and S. Liu, *Energy Environ. Sci.*, 2017, **10**, 2095–2102.
17 D. H. Cao, C. C. Stoumpos, O. K. Farha, J. T. Hupp and M. G. Kanatzidis, *J. Am. Chem. Soc.*, 2015, **137**, 7843–7850.
18 K. Lee, J. Ryu, H. Yu, J. Yun, J. Lee and J. Jang, *Nanoscale*, 2017, **9**, 16249–16255.

19 C.-T. Lin, S. Pont, J. Kim, T. Du, S. Xu, X. Li, D. Bryant, M. A. Mclachlan and J. R. Durrant, *Sustainable Energy Fuels*, 2018, **2**, 1686–1692.
20 A. K. Jena, Y. Numata, M. Ikegami and T. Miyasaka, *J. Mater. Chem. A*, 2018, **6**, 2219–2230.
21 T. Leijtens, E. Eperon, S. Pathak, A. Abate, M. M. Lee and H. J. Snaith, *Nat. Commun.*, 2013, **4**, 2885.
22 D. D. Girolamo, F. D. Giacomo, F. Matteocci, A. G. Marrani, D. Dini and A. Abate, *Chem. Sci.*, 2020, **11**, 7746–7759.
23 X. Yin, Y. Guo, H. Xie, W. Que and L. B. Kong, *Sol. RRL*, 2019, **3**, 1900001.
24 C. Liu, W. Li, J. Chen, J. Fan, Y. Mai and R. E. I. Schropp, *Nano Energy*, 2017, **41**, 75–83.
25 J. You, L. Meng, T.-B. Song, T.-F. Guo, Y. Yang, W.-H. Chang, Z. Hong, H. Chen, H. Zhou, Q. Chen, Y. Liu, N. D. Marco and Y. Yang, *Nat. Nanotechnol.*, 2016, **11**, 75–81.
26 Z. Liu, J. Chang, Z. Lin, L. Zhou, Z. Yang, D. Chen, C. Zhang, S. Liu and Y. Hao, *Adv. Energy Mater.*, 2018, **8**, 1703432.
27 P. Zhang, J. Wu, T. Zhang, Y. Wang, D. Liu, H. Chen, L. Ji, C. Liu, W. Ahmad, Z. D. Chen and S. Li, *Adv. Mater.*, 2018, **30**, 1703737.
28 Q. Jiang, L. Zhang, H. Wang, X. Yang, J. Meng, H. Liu, Z. Yin, J. Wu, X. Zhang and J. You, *Nat. Energy*, 2017, **2**, 16177.
29 C. Liu, W. Li, C. Zhang, Y. Ma, J. Fan and Y. Mai, *J. Am. Chem. Soc.*, 2018, **140**, 3825–3828.
30 A. D. Z. Mendaza, A. Melianas, S. Rossbauer, O. Backe, L. Nordstierna, P. Erhart, E. Olsson, T. D. Anthopoulos, O. Inganas and C. Muller, *Adv. Mater.*, 2015, **27** 7325–7331.
31 C. Xu, Z. Liu and E.-C. Lee, *J. Mater. Chem. C*, 2019, **7**, 6956–6963.
32 H.-S. Lin, I. Jeon, R. Xiang, S. Seo, J.-W. Lee, C. Li, A. Pal, S. Manzhos, M. S. Goorsky, Y. Yang, S. Maruyama and Y. Matsuo, *ACS Appl. Mater. Interfaces*, 2018, **10**, 39590–39598.
33 P. Liu, N. Han, W. Wang, R. Ran, W. Zhou and Z. Shao, *Adv. Mater.*, 2021, **33**, 2002582.
34 R. Liu, Y. Yu, T. Hu, F. Zhang, C. Liu, H. Hou, M. Zhang, X. Chen and H. Yu, *J. Power Sources*, 2021, **512**, 230452.
35 A. Caiazzo, K. Datta, J. Jiang, M. C. Gélvez-Rueda, J. Li, R. Ollearo, J. M. Vicent-Luna, S. Tao, F. C. Grozema, M. M. Wienk and R. A. J. Janssen, *Adv. Energy Mater.*, 2021, **11**, 2102144.
36 C. Bi, Q. Wang, Y. Shao, Y. Yuan, Z. Xiao and J. Huang, *Nat. Commnun.*, 2015, **6**, 7747.
37 F. Wang, T. Zhang, Y. Wang, D. Liu, P. Zhang, H. Chen, L. Ji, L. Chen, Z. D. Chen, J. Wu, X. Liu, Y. Li, Y. Wang and S. Li, *J. Mater. Chem. A*, 2019, **7**, 12166–12175.
38 Z. Liu and E.-C. Lee, *Sustainable Energy Fuels*, 2021, **5**, 2354–2361.
39 H. Wei, J. Xiao, Y. Yang, S. Lv, J. Shi, X. Xu, J. Dong, Y. Luo, D. Li and Q. Meng, *Carbon*, 2015, **93**, 861–868.
40 T. T. Tong, X. H. Li, S. H. Guo, J. Han and B. Q. Wei, *Nano Energy*, 2017, **41**, 591–599.
41 E. Widianto, Shobih, E. S. Rosa, K. Triyana, N. M. Nursam and I. Santoso, *Opt. Mater.*, 2021, **121**, 111584.
42 Y. Liu, Z. Liu and E.-C. Lee, *ACS Appl. Energy Mater.*, 2019, **2**, 1932–1942.
43 Z. Liu, P. You, C. Xie, G. Tang and F. Yan, *Nano Energy*, 2016, **28**, 151–157.